Chapter 22
Heteronuclear Shift Correlation Spectroscopy

Thomas T. Nakashima and R. E. D. McClung

Gunning/Lemieux Chemistry Centre, Department of Chemistry, Room E3-24, University of Alberta, Edmonton, Alberta T6G 2G2, Canada

22.1 INTRODUCTION

Heteronuclear shift correlation spectroscopy is the name given to a class of two-dimensional NMR experiments (see Chapter 2) that generate contour maps in which the chemical shifts of two distinct types of nuclei (hence the designation "hetero") are correlated.[1–8] Acronyms for heteronuclear shift correlation spectroscopy include HETCOR, HSC, Hetero-COSY, H-C COSY, and H-X COSY. Although the examples described below involve $^{1}H-^{13}C$ heteronuclear shift correlation, heteronuclear shift correlation maps may be obtained for any pair of nuclei which are connected by scalar spin–spin coupling.[2] (See also Chapters 12 and 27.)

The most fundamental problem in the application of NMR spectroscopy to the elucidation of molecular structures is the assignment of the observed resonances in the NMR spectra to the specific atoms in the molecule. An essential component of the assignment process for ^{13}C spectra is the determination of the number of protons that are directly bonded to a given carbon atom (i.e., finding out whether a particular carbon resonance corresponds to a CH, CH_2, CH_3, or quaternary carbon). The task of assigning the peaks in NMR spectra, particularly in ^{13}C spectra, has been simplified by a number of developments over the past 30 years. The simple natural abundance ^{13}C spectrum of a molecule will show a single resonance line for each quaternary carbon atom, a 1:1 doublet for each CH carbon, a 1:2:1 triplet for each CH_2, and a 1:3:3:1 quartet for each CH_3 carbon atom, with separations of about 120–180 Hz between the various multiplet lines. The spacing here is equal to the carbon–proton coupling constant, $^{1}J_{CH}$. This simple spectrum has inherent low sensitivity, and the large spacing between multiplet lines results in considerable overlapping of the resonances from different carbon atoms. The ^{13}C spectrum obtained with broadband ^{1}H decoupling has much higher sensitivity, but contains no multiplet structure to aid in the assignment process. The introduction of single frequency off-resonance proton decoupling (SFORD) retained the multiplet structure of the simple ^{13}C spectrum (but with considerably smaller multiplet line separations) and much of the sensitivity of the ^{1}H-decoupled spectrum, but the overlapping of peaks in crowded regions of the SFORD spectrum often prevented unambiguous assignment of the peaks.[9]

With the development of FT NMR spectrometers allowing facile control of rf pulse lengths and phases on both observe and decoupler channels, a number of experiments were developed to determine the number of protons attached to a particular carbon atom. The INEPT and DEPT sequences involve the transfer of proton magnetization to carbon.[10–12] One obtains increased sensitivity with INEPT and DEPT, and these sequences (with a refocusing period after the magnetization transfer step) yield proton-decoupled carbon spectra with distinguishable responses from CH, CH_2, and CH_3 carbons, but no responses from quaternary carbons. Another very important tool for assigning the number of protons attached to each carbon in the molecule is the APT experiment, which gives $^{13}C\{^1H\}$ spectra in which all quaternary and CH_2 carbons give peaks with positive phase, and all CH and CH_3 carbons give peaks with negative phase.[10–12] The INEPT, DEPT, and APT experiments are excellent analytical tools for determining the number of protons attached to a particular carbon atom, but do not connect the peaks in the ^{13}C and ^1H spectra to give confirmed assignments of resonances.

Selective ^1H-decoupled experiments were developed to identify the carbon atom to which a particular proton is attached. The identification of carbon and hydrogen atoms that are directly bonded to each other is invaluable in making unambiguous assignments of all resonance lines in both ^{13}C and ^1H spectra. In selective ^1H decoupling, the resonance of a particular proton is selectively irradiated during the acquisition of the ^{13}C spectrum, and one observes a single sharp line for the carbon atom to which the irradiated protons are directly bonded. Selective ^1H-decoupling experiments are of limited utility when the region to be decoupled in the proton spectrum is crowded, or when there are nonequivalent methylene protons which cannot be decoupled simultaneously. The $^1H-^{13}C$ heteronuclear shift correlation experiment has revolutionized the ease with which one can correlate the ^{13}C resonance for each carbon atom in the molecule to the ^1H resonances of the protons that are directly attached to that carbon atom. Furthermore, since heteronuclear correlation involves the transfer of proton magnetization to carbon, the recycling times between accumulations are determined by proton relaxation times which are usually shorter than those for carbon, and one obtains enhanced signal intensity due to the larger proton magnetization which is transferred to carbon. Both of these features lead to a sensitivity enhancement relative to normal ^{13}C spectroscopy.[1–8]

In this chapter, we shall describe the basic principles involved in heteronuclear shift correlation experiments, the important features that have been developed to simplify the correlation maps, and modifications that have been introduced to improve the sensitivity and expand the utility of heteronuclear shift correlation.

22.2 BASIC PRINCIPLES

As a typical example, the $^1H-^{13}C$ shift correlation map for sucrose is shown in Figure 22.1. The proton chemical shifts are identified in the ^1H spectrum along the vertical axis (often referred to as the f_1 dimension), and the carbon chemical shifts in the ^{13}C spectrum along the horizontal axis (the f_2 dimension), and the peaks in the contour map identify all directly bonded H and C atoms in the sucrose molecule. There is considerable congestion in the ^1H NMR spectrum (six proton resonances within the interval 3.6–4.0 ppm), but the peaks in the ^{13}C spectrum are well separated. Hence, the peaks in the 2D shift correlation map are all well resolved, so that, if the assignments of the carbon resonances are known then the assignments of the proton spectrum follow directly.

22.2.1 The Basic Heteronuclear Correlation Experiment

The basic principles involved in heteronuclear shift correlation experiments[1,2] are best understood by considering the pulse sequence shown in Figure 22.2(a). For completeness, the product operator transformations for the CH spin system during each of the steps are also included in the following description.[13] Proton and carbon nuclear spins are designated I and S, respectively. Heteronuclear correlation spectroscopy involves the following basic elements.

1. A broadband 90° ^1H pulse rotates the proton z magnetizations into the transverse plane (in product operator terms, $\hat{I}_z \rightarrow \hat{I}_y$).
2. The transverse proton magnetizations precess and become "labeled" with their chemical shift frequencies (ν_H) during a precession period of incremented length t_1. The protons interact with

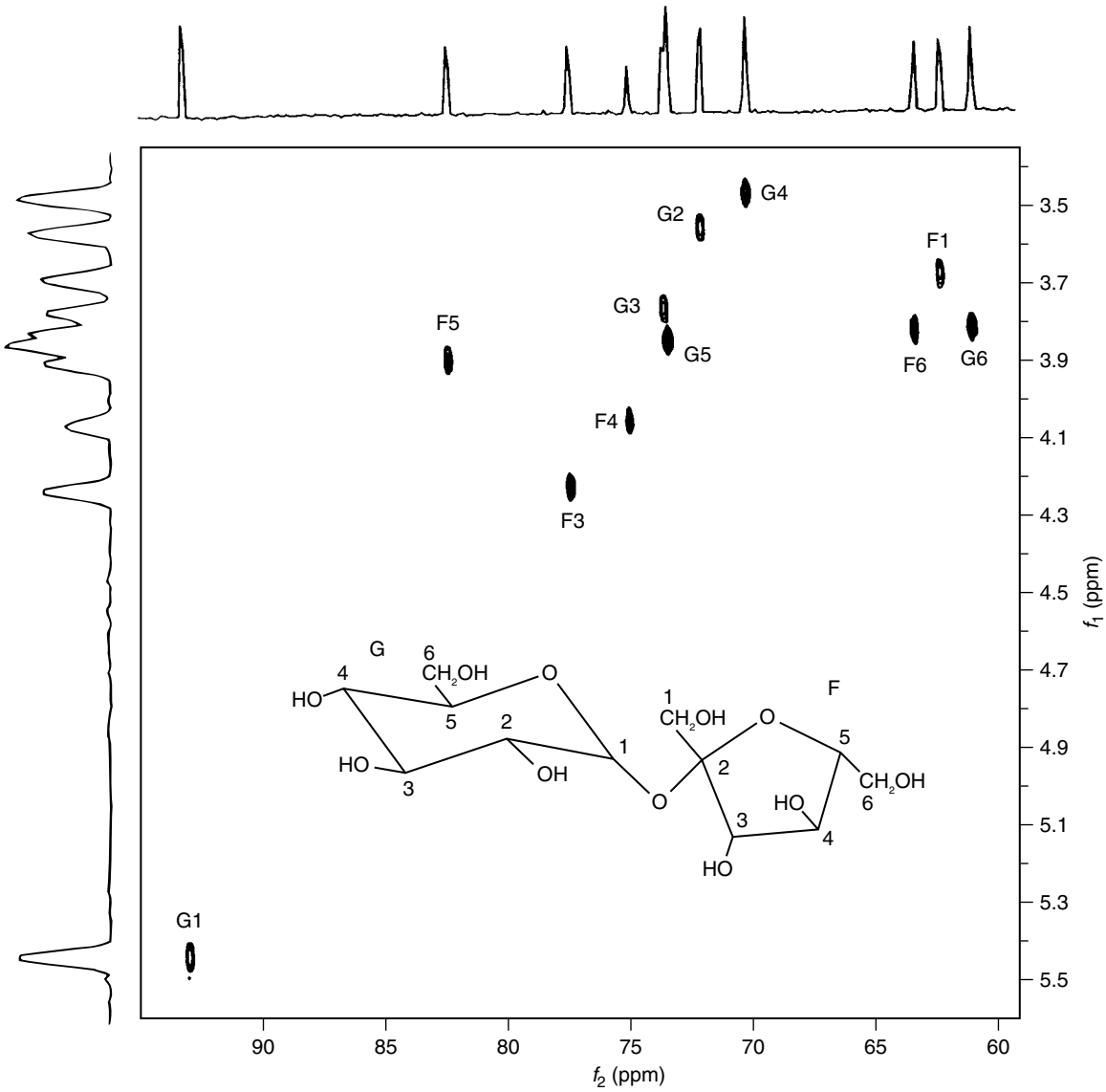

Figure 22.1. Conventional heteronuclear shift correlation map for sucrose in D_2O (10 mg in $\approx$ 0.5 mL) at 500 MHz obtained with the pulse sequence in Figure 22.2(d) ($^{13}C-^{1}H$ and $^{1}H-^{1}H$ decoupled in f_1, $^{13}C-^{1}H$ decoupled in f_2).

the ^{13}C nuclei via scalar spin–spin coupling during this labeling period, and antiphase proton magnetizations are generated by these interactions. [$\hat{I}_y \rightarrow 2\hat{I}_x\hat{S}_z\cos(2\pi\nu_H t_1)\sin(\pi\ ^1J_{CH}t_1)$.]

3. The application of simultaneous broadband 90° pulses to both ^{13}C and ^{1}H nuclei converts the antiphase proton magnetizations into antiphase carbon magnetizations. [$2\hat{I}_x\hat{S}_z\cos(2\pi\nu_H t_1)\sin(\pi\ ^1J_{CH}t_1) \rightarrow 2\hat{I}_z\hat{S}_y\cos(2\pi\nu_H t_1)\sin(\pi\ ^1J_{CH}t_1)$.]
4. These antiphase carbon magnetizations precess, are labeled with their chemical shift frequencies (ν_C), and $^{13}C-^{1}H$ spin–spin interactions

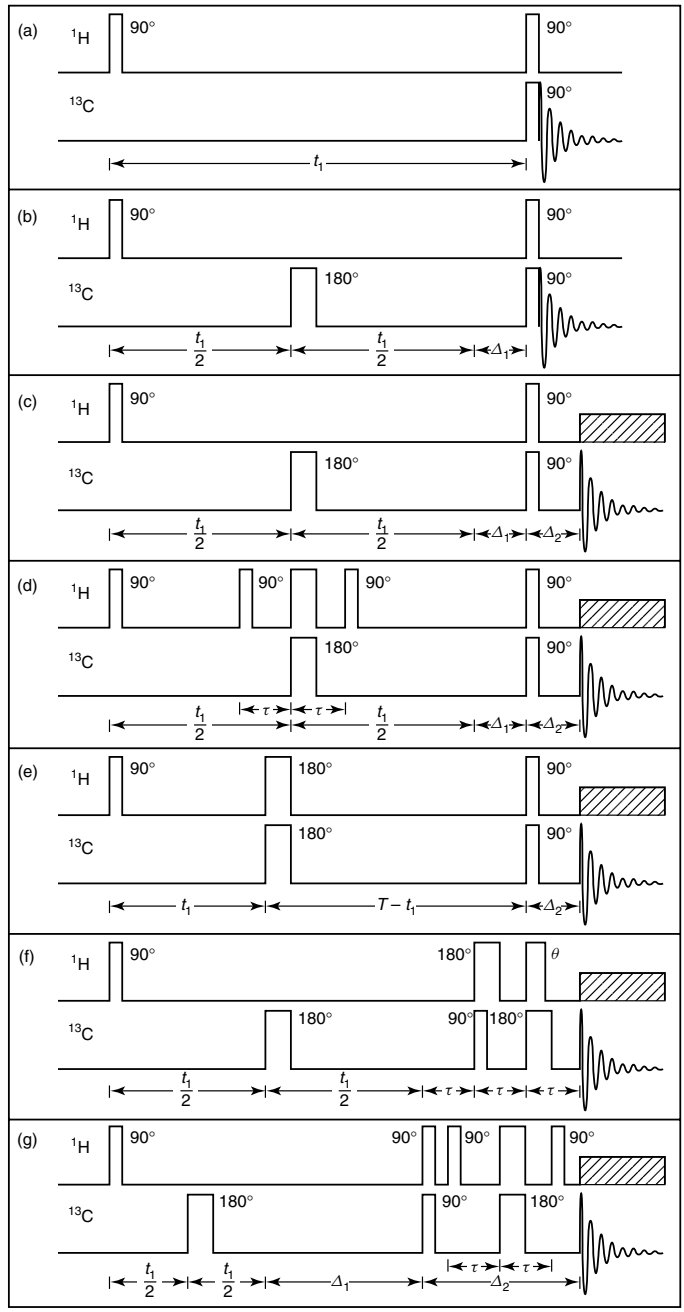

Figure 22.2. Heteronuclear shift correlation pulse sequences: (a) basic sequence with no decoupling; (b) sequence with ^{13}C–^{1}H decoupling in f_1; (c) sequence with ^{13}C–^{1}H decoupling in f_1 and f_2; (d) sequence with ^{13}C–^{1}H decoupling in f_1 and in f_2 and ^{1}H–^{1}H decoupling in f_1; (e) sequence using constant evolution time T; (f) sequence with DEPT magnetization transfer for multiplet selective editing; (g) sequence for detection of long range correlations. In sequences (c)–(e), $\Delta_1 = 1/(2\,{}^1J_{CH})$ and $\Delta_2 \approx 1/(3\,{}^1J_{CH})$. In sequence (g), $\Delta_1 = 1/(2J_{CH}^{\text{long range}})$ and $\Delta_2 \approx 1/(3J_{CH}^{\text{long range}})$. $\tau = 1/(2\,{}^1J_{CH})$ in sequences (d), (f), and (g).

produce in-phase carbon magnetizations, which are sampled at times t_2 during the detection period. [$2\hat{I}_z\hat{S}_y\cos(2\pi\nu_H t_1)\sin(\pi\,{}^1J_{CH}t_1) \rightarrow -\hat{S}_x\cos(2\pi\nu_C t_2)\sin(\pi\,{}^1J_{CH}t_2)\cos(2\pi\nu_H t_1)\sin(\pi\,{}^1J_{CH}t_1)$.]

5. Fourier transformation of the magnetization data yields a contour map that contains peaks connecting the chemical shift (ν_H) of each proton to the chemical shift (ν_C) of the carbon to which it is directly bonded.

The heteronuclear shift correlation map for sucrose shown in Figure 22.3 was generated using this basic pulse sequence given in Figure 22.2(a), and differs in two important respects from the map shown in Figure 22.1 obtained with the sequence in Figure 22.2(d)—the correlation map in Figure 22.3 shows $^{13}C-{}^1H$ spin–spin multiplets in both the f_1 (proton) and f_2 (carbon) dimensions, while $^{13}C-{}^1H$ couplings are absent in both dimensions and $^1H-{}^1H$ couplings are absent in the f_1 dimension of the map shown in Figure 22.1. A CH_3 group gives a correlation profile consisting of eight peaks (two quartets with intensities 1:1:−1:−1 in the carbon dimension at proton frequencies $\nu_H \pm {}^1/_2\,{}^1J_{CH}$), a CH_2 group gives four peaks (two 1:0:−1 triplets), and a CH group gives four peaks (two 1:−1 doublets). The antiphase nature of the multiplets in the carbon dimension is very undesirable, since it does not permit proton decoupling during acquisition, and the presence of $^{13}C-{}^1H$ splitting of the profiles in both proton and carbon dimensions is undesirable, since the primary interest here is in chemical shifts, not in spin–spin couplings. Modification of this basic experiment allows decoupling in both dimensions as described below.

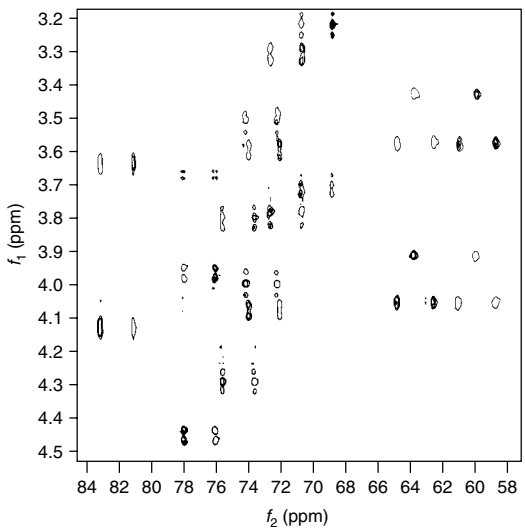

Figure 22.3. A portion of the heteronuclear shift correlation map for a concentrated solution of sucrose in D_2O at 300 MHz (^1H), with no decoupling in either dimension. Obtained with pulse sequence in Figure 22.2(a). Multiple contours represent positive peaks, single contours are negative peaks.

22.2.2 Carbon-13 Decoupling in f_1

The $^{13}C-{}^1H$ couplings can be removed from the f_1 (proton) dimension of the heteronuclear shift correlation map by inserting a 180° carbon pulse in the center of the t_1 labeling period,[2] and adding a delay of length $\Delta_1 = 1/(2\,{}^1J_{CH})$ before the proton and carbon 90° pulses are applied as shown in Figure 22.2(b). The effect of the 180° carbon pulse is to remove the effects of $^{13}C-{}^1H$ coupling during the labeling period [$\hat{I}_y \rightarrow \hat{I}_y\cos(2\pi\nu_H t_1) - \hat{I}_x\sin(2\pi\nu_H t_1]$, and the delay Δ_1 must be added to allow spin–spin coupling to transform the in-phase proton magnetization into antiphase magnetization ($\hat{I}_y\cos(2\pi\nu_H t_1) \rightarrow -2\hat{I}_x\hat{S}_z\cos[2\pi\nu_H(t_1 + \Delta_1)]$ and $\hat{I}_x\sin(2\pi\nu_H t_1) \rightarrow 2\hat{I}_y\hat{S}_z\sin\,2\pi\nu_H(t_1 + \Delta_1)]$) so that it may be converted to antiphase carbon magnetization by the 90° pulses. The addition of the Δ_1 delay introduces phase differences between the final signals from the different proton–carbon moieties in the molecule, so phase-sensitive correlation maps are not obtained.

22.2.3 ^1H Decoupling in f_1

The 90° carbon and proton pulses in all heteronuclear shift correlation pulse sequences convert *antiphase* proton magnetization ($\hat{I}_x\hat{S}_z$ or $\hat{I}_y\hat{S}_z$) into *antiphase* carbon magnetization ($\hat{I}_z\hat{S}_y$ or $\hat{I}_z\hat{S}_x$). If one turns on the proton decoupler immediately after these pulses, no signals will be acquired, since only *in-phase* carbon magnetization is detected. Hence, in order to effect proton decoupling during the t_2 acquisition period, one must introduce a delay of length Δ_2 between the 90° pulses and the acquisition to allow $^{13}C-{}^1H$ coupling to convert *antiphase* into

in-phase magnetization ($\hat{I}_z\hat{S}_y \rightarrow -[\hat{S}_x\cos(\nu_C\Delta_2) + \hat{S}_y\sin(\nu_C\Delta_2)]\sin(\pi\ ^1J_{CH}\Delta_2)$), as shown in the pulse sequence in Figure 22.2(c). When the decoupler is turned on at the end of Δ_2, a proton-decoupled carbon spectrum will be acquired and displayed in the f_2 dimension of the heteronuclear shift correlation map.[2] The relative magnitudes of the detected signals for CH, CH_2, and CH_3 groups are proportional to $\sin(\pi\ ^1J_{CH}\Delta_2)$, $\sin(2\pi\ ^1J_{CH}\Delta_2)$, and $\sin(\pi\ ^1J_{CH}\Delta_2) + \sin(3\pi\ ^1J_{CH}\Delta_2)$, respectively. This dependence on the magnitude of Δ_2 implies that no single value of Δ_2 will give maximum signal amplitudes for all CH_n moieties. Instead, one should use a value $\Delta_2 \approx 1/(3\ ^1J_{CH})$ in order to obtain carbon signals of approximately equal magnitude for all spin systems.

22.2.4 Elimination of $^1H-^1H$ Couplings in f_1

The presence of $^1H-^1H$ couplings in the f_1 dimension of the heteronuclear shift correlation map needlessly complicates and lowers the overall intensity of the correlation peaks. These couplings arise from spin–spin interactions between the proton(s) in a $^{13}C-^1H_n$ fragment ("directly bonded" protons) and the protons in neighboring $^{12}C-^1H_{n'}$ fragments ("remote" protons). (The 1.1% natural abundance of ^{13}C nuclei means that the neighboring carbon atoms in the molecular skeleton will be ^{12}C in over 98% of the molecules.) These couplings can be removed by selectively inverting the magnetizations of the remote protons in the center of the t_1 labeling period without inverting the magnetizations of the directly bonded protons.[2] This selective manipulation of the remote protons can be effected using bilinear rotational decoupling (BIRD), which consists of the following sequence:[2,6–8]

$$90^\circ_{x^1H} - 1/(2^1J_{CH}) - 180^\circ_{^{13}C},\ 180^\circ_{y^1H} - 1/(2^1J_{CH}) - 90^\circ_{x^1H} \quad (22.1)$$

as shown in the heteronuclear shift correlation sequence in Figure 22.2(d). This sequence gives heteronuclear shift correlation maps with $^1H-^1H$ decoupling in f_1, and is the sequence used to obtain the heteronuclear shift correlation map for sucrose given in Figure 22.1.

The operation of this BIRD sequence is easily understood by following the evolution of the magnetization components of the directly bonded and remote protons as shown in Figure 22.4. The y components of the magnetizations of both directly bonded and remote protons are converted to z magnetizations by the

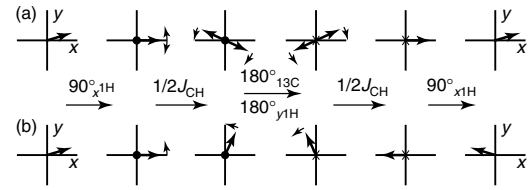

Figure 22.4. Behavior of transverse magnetization components for directly bonded (a) and remote (b) protons during BIRD. Symbols • and × at the origin of coordinates indicate positive and negative z components, respectively.

$90^\circ_{x^1H}$ pulse, are then inverted by the $180^\circ_{y^1H}$ pulse, and are finally rotated by the final $90^\circ_{x^1H}$ pulse so that they again lie along the y axis. The x components of the magnetizations of remote and directly bonded protons are not affected by the $90^\circ_{x^1H}$ pulse, but behave differently during the precession periods since only the directly bonded protons experience C–H coupling during these periods. The precession of the x components of the magnetizations of remote protons due to their different chemical shifts during the first $1/(2^1J_{CH})$ delay period is reversed during the delay following the $180^\circ_{y^1H}$ pulse, so that the magnetizations are refocused along the negative x axis just before the final $90^\circ_{x^1H}$ pulse is applied. Thus, the effect of the BIRD element on the transverse magnetization of remote protons [see Figure 22.4(b)] is equivalent to that of a 180°_y pulse ($M_y \rightarrow M_y$ and $M_x \rightarrow -M_x$). On the other hand, C–H coupling causes the x magnetizations of directly bonded protons to precess as two separate components (one component precessing at frequency $\nu_H + {}^1/_2\ ^1J_{CH}$ and one at $\nu_H - {}^1/_2\ ^1J_{CH}$). The $180^\circ_{^{13}C}$ and $180^\circ_{y^1H}$ pulses cause the chemical shift precession during the first delay period to be reversed during the second $1/(2^1J_{CH})$ delay period, and the two components of the magnetization ultimately come together and lie along the positive x direction when the final $90^\circ_{x^1H}$ pulse is applied. Hence, as shown in Figure 22.4(a), the BIRD element has no net effect on the magnetizations of directly bonded protons ($M_y \rightarrow M_y$ and $M_x \rightarrow M_x$). The "extra" 180° rotation that the magnetizations of directly bonded protons experience is, in fact, a result of the *bilinear* rotation due to $^1H-^{13}C$ coupling during the two $1/(2^1J_{CH})$ delay periods of the BIRD sequence.

An alternate approach to removing $^1H-^1H$ couplings in f_1 is directly analogous to that employed in decoupled COSY, and uses a pulse sequence with a constant evolution time T as shown in

Figure 22.2(e)[3,6] (see Chapter 12). In this sequence, the time at which simultaneous $180^\circ_{^1\mathrm{H}} - 180^\circ_{^{13}\mathrm{C}}$ pulses are applied is "stepped across" the evolution period from time 0 to time T in increments of T/n_1 for successive values of t_1. Here, n_1 is the total number of t_1 values. This sequence has serious drawbacks, since T must be an odd multiple of $1/(2^1J_{\mathrm{CH}})$ for maximum polarization transfer to carbon and maximum sensitivity. If T is long, small variations in $^1J_{\mathrm{CH}}$ among the various CH_n fragments in the molecule lead to variations of unacceptable magnitude in the intensities of peaks in the heteronuclear shift correlation map. It has been suggested that T be set equal to 0.02 s, but this restricts the resolution in f_1 to 50 Hz point^{-1}.

22.2.5 Practical Considerations

In order to obtain heteronuclear correlation maps free of instrumental artifacts, one must use rf pulses whose lengths have been carefully calibrated, and cycle the phases of the pulses in an appropriate fashion as detailed in the following sections.

22.2.5.1 Pulse Width Calibration

One must calibrate the lengths of the pulses on both "observe" (carbon) and "decoupler" (proton) rf channels. One should use a sample with a short carbon relaxation time T_1, and a sufficiently strong ^{13}C signal that a single transient produces a spectrum of high signal-to-noise ratio [an approx. 60:40 $CHCl_3$:$CDCl_3$ mixture doped with tris(acetylacetonato)chromium(III) is suitable].

Calibration of pulse lengths for the "observe" channel is straightforward: set the transmitter frequency close to the exact resonance for the sample in order to avoid off-resonance effects; and generate a series of "one pulse" proton-decoupled carbon spectra with the carbon pulse length increased by a small amount in successive spectra (being sure to use a relaxation delay $\geq 3T_1$ between the experiments). The spectrum with lowest signal amplitude (the "null") corresponds to a 180° pulse, and the 90° pulse length is half of this value. If a poor null is obtained, the probe has significant $\boldsymbol{B}_1$ inhomogeneity. If the signal amplitude varies in a sinusoidal fashion with pulse length, but is skewed toward the shorter pulse lengths, the sequence of experiments should be repeated with a longer relaxation delay.

Calibration of pulse lengths for the decoupler channel is more complicated, since the effects of proton pulses must be observed indirectly. One method for determining the 90° pulse length for protons is to perform a series of experiments using the pulse sequence

$$90^\circ_{^{13}\mathrm{C}} - 1/(2^1J_{\mathrm{CH}}) - 180_{^{13}\mathrm{C}},\ \theta_{^1\mathrm{H}} - 1/(2^1J_{\mathrm{CH}}) - \text{acquire } ^{13}\mathrm{C} \text{ with } ^1\mathrm{H} \text{ decoupling} \tag{22.2}$$

with the length of the proton θ pulse increased by a small increment in successive experiments.[5] In these experiments, it is important to set the transmitter frequencies close to exact resonance. The spectrum with minimum signal corresponds to $\theta = 90^\circ$.

22.2.5.2 Phase Cycling and Coherence Pathway Selection

In order to avoid the appearance of instrumental artifacts and other undesirable features in heteronuclear shift correlation maps, it is important to cycle the phases of the pulses and the detector in an appropriate manner.[14] The principles of phase cycling are deeply rooted in the concepts of coherence levels and the coherence pathways that the magnetization of the spin system follows from excitation to detection. In simple terms, one can classify time-coherent properties of a spin system by the Zeeman frequencies with which they rotate about the applied magnetic field $\boldsymbol{B}_0$. For example, in the ^{13}C–^{1}H spin system, the longitudinal magnetizations (product operators $\hat{I}_z$ and $\hat{S}_z$) do not rotate about $\boldsymbol{B}_0$, and are therefore coherences of level 0; transverse magnetizations ($\hat{I}_x \pm \mathrm{i}\hat{I}_y$ and $\hat{S}_x \pm \mathrm{i}\hat{S}_y$) rotate at frequencies $\pm\nu_{\mathrm{C}}$ or $\pm\nu_{\mathrm{H}}$ about $\boldsymbol{B}_0$, and belong to coherence levels +1 and −1; zero quantum coherences ($2\hat{I}_x\hat{S}_x + 2\hat{I}_y\hat{S}_y$ and $2\hat{I}_x\hat{S}_y - 2\hat{I}_y\hat{S}_x$) rotate at frequencies $\pm(\nu_{\mathrm{H}} - \nu_{\mathrm{C}})$, and belong to coherence level 0; while double quantum coherences ($2\hat{I}_x\hat{S}_x - 2\hat{I}_y\hat{S}_y$ and $2\hat{I}_x\hat{S}_y + 2\hat{I}_y\hat{S}_x$) rotate at frequencies $\pm(\nu_{\mathrm{H}} + \nu_{\mathrm{C}})$, and are coherences of level +2 and −2. In all FT NMR experiments, the spin system begins with longitudinal magnetization in coherence level 0 and ends with the sampling of in-phase transverse magnetization in the −1 coherence level. The trajectory that the magnetization follows during the course of the experiment defines a coherence pathway.

The coherence level of a spin system can be changed by the application of an rf pulse, but does not change during a period of free precession. When a pulse with phase angle ϕ with respect to the x axis of the rotating frame causes a change from

coherence level p_1 to coherence level p_2, a phase factor $\exp[-i(p_2 - p_1)\phi]$ becomes incorporated into the resulting coherence. For example, the application of a 90° proton pulse with phase ϕ to longitudinal proton magnetization (coherence level 0) produces a +1 coherence ($\hat{I}_x + i\hat{I}_y$) with phase factor $\exp(-i\phi)$, and a −1 coherence ($\hat{I}_x - i\hat{I}_y$) with phase factor $\exp(i\phi)$. If the proton signal were acquired at this point, a receiver phase factor of $\exp(i\phi)$ would be applied to the detected −1 coherence during acquisition so that the final signal is independent of ϕ. In heteronuclear shift correlation experiments where there are many pulses whose phases may vary during spectral accumulation, the phases of the pulses and detector must be varied in concert in order to select only signals derived from coherences that have followed the desired coherence pathway(s), and suppress undesirable features.

Three possible coherence pathways for signals that can be observed in the heteronuclear shift correlation experiment are shown in Figure 22.5. The signals associated with these pathways have phase factors $\exp[i(-\phi_1 + \phi_2 + \phi_3)]$ (solid line), $\exp(i\phi_3)$ (dashed line), and $\exp[i(\phi_1 - \phi_2 + \phi_3)]$ (dotted line). The solid pathway is followed by proton magnetization ($\hat{I}_z$), which is converted into coherence of level +1 $[(\hat{I}_x + i\hat{I}_y)\exp(-i\phi_1)]$ by the proton $90^\circ_{\phi_1}$ pulse, and is frequency-labeled during the t_1 evolution [a factor $\exp(-2i\pi\nu_H t_1)$ is incorporated into the coherence]; the +1 coherence passes to coherence level 0 when the proton $90^\circ_{\phi_3}$ pulse is applied, is converted to antiphase transverse carbon magnetization of coherence level −1 by the carbon $90^\circ_{\phi_3}$ pulse, and ultimately gives peaks at ($-\nu_H$, ν_C) on the 2D contour map. The dotted pathway is followed by proton magnetization ($\hat{I}_z$), which is converted into coherence of level −1 $[(\hat{I}_x - i\hat{I}_y)\exp(i\phi_1)]$ by the proton $90^\circ_{\phi_1}$ pulse, and is frequency-labeled during the t_1 evolution [a factor $\exp(2i\pi\nu_H t_1)$ is incorporated]; this −1 coherence passes through the zero coherence level when the proton $90^\circ_{\phi_1}$ pulse is applied, is converted to antiphase transverse carbon magnetization of coherence level −1 by the carbon $90^\circ_{\phi_3}$ pulse, and gives peaks at (ν_H, ν_C). The dashed pathway is followed by carbon magnetization ($\hat{S}_z$), which is not affected by the proton pulses, is converted into observable transverse magnetization $[(\hat{S}_x - i\hat{S}_y)\exp(i\phi_3)]$ by the carbon $90^\circ_{\phi_3}$ pulse, and gives peaks at (0, ν_C). By setting the phase angle, ϕ_R, of the detector equal to $\phi_1 - \phi_2 + \phi_3$, appending the phase factor $\exp(-i\phi_R)$ to each of the signals as they are accumulated, and cycling the phases ϕ_1, ϕ_2, and ϕ_3 independently through values 0°–90°–180°–270°, the final spectrum will be that for spins that have followed the dotted pathway shown in Figure 22.5. This phase cycling suppresses signals arising from spins that have traversed the solid and dashed coherence pathways. This cycling of the phases of pulses and detector is very important, since it removes "zero-frequency" artifacts (dashed coherence pathway) from the heteronuclear shift correlation map, and allows one to place the proton transmitter frequency at the center of the spectrum and achieve quadrature detection in f_1, since the "quad image" peaks (solid coherence pathway) at ($-\nu_H$, ν_C) are suppressed.

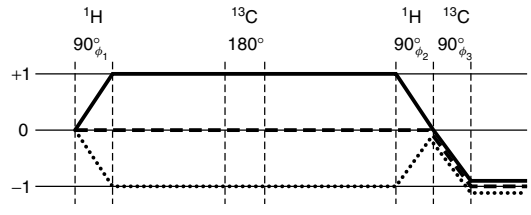

Figure 22.5. Coherence pathways involved in the basic heteronuclear shift correlation experiment. Pathways followed by desired signals (. . .), 'quad' images (—), and carbon magnetization (- -) are shown.

22.3 ADVANCEMENTS IN HETERONUCLEAR SHIFT CORRELATION AND RELATED EXPERIMENTS

There have been a number of advances and extensions of heteronuclear shift correlation that afford spectral editing,[3] selection of long-range rather than directly bonded correlations,[3,5–7,15] increased sensitivity, and solvent suppression using inverse detection and multiple quantum filtering techniques.[1,3,16–19] A summary of the important features of these advances is given in the following sections.

22.3.1 Spectral Editing

In order to remove ambiguities from congested heteronuclear shift correlation maps, it is sometimes useful to display selectively only the correlations for CH, CH_2, or CH_3 fragments.[3] In principle, this might be done by taking linear combinations of a set of correlation maps generated with the pulse sequence in

Figure 22.2(c) or (d) using a set of suitably chosen values of Δ_2. It is, however, more efficient to use the 2D DEPT sequence shown in Figure 22.2(f), because the editing capability of this sequence is less sensitive to variations in $^1J_{CH}$. The evolution part of the heteronuclear shift correlation sequence is unchanged, but the transfer of magnetization from proton to carbon is now based on DEPT rather than INEPT, and involves zero and double quantum coherences.[11] The editing of heteronuclear shift correlation maps according to the number of attached protons is based on the variation of the intensities of the carbon signals with the flip angle θ for the final proton pulse in the DEPT transfer:

$$I_{CH} = \sin\theta \tag{22.3}$$

$$I_{CH_2} = \sin 2\theta \tag{22.4}$$

$$I_{CH_3} = 3(\sin\theta + \sin 3\theta)/4 \tag{22.5}$$

One collects FIDs for three values of θ—FID(θ_1), FID(θ_2), and FID(θ_3)—and constructs linear combinations of these FIDs that selectively enhance each of the CH_n moieties:

$$\left.\begin{aligned} \theta_1 = 45^\circ, \quad \theta_2 = 90^\circ, \quad \theta_3 = 135^\circ \\ \mathrm{FID_{CH}} = \mathrm{FID}(90^\circ), \\ \mathrm{FID_{CH_2}} = \mathrm{FID}(45^\circ) - \mathrm{FID}(135^\circ), \\ \mathrm{FID_{CH_3}} = \mathrm{FID}(45^\circ) + \mathrm{FID}(135^\circ) - 0.707\,\mathrm{FID}(90^\circ), \end{aligned}\right\}$$

$$\left.\begin{aligned} \theta_1 = 30^\circ, \quad \theta_2 = 90^\circ, \quad \theta_3 = 150^\circ \\ \mathrm{FID_{CH}} = \mathrm{FID}(90^\circ) \\ \mathrm{FID_{CH_2}} = \mathrm{FID}(30^\circ) - \mathrm{FID}(150^\circ) \\ \mathrm{FID_{CH_3}} = \mathrm{FID}(30^\circ) + \mathrm{FID}(150^\circ) - \mathrm{FID}(90^\circ) \end{aligned}\right\} \tag{22.6}$$

An example of the editing effectiveness of 2D DEPT is shown in Figure 22.6, where the CH and CH_2 maps for cholesterol are compared with the heteronuclear shift correlation map containing peaks from all CH_n fragments. The unedited map [Figure 22.6(a)] shows four strong methyl resonances which are suppressed in the edited maps shown in Figures 22.6(b) and (c). The region near $\delta_C = 35$ ppm in the unedited map shows several overlapping peaks, which are resolved into two CH_2 correlations and one CH correlation in the edited maps.

22.3.2 Heteronuclear Correlations Based on Long-Range ^{1}H–^{13}C Couplings

One of the most important NMR methods used in structural elucidation of complex organic molecules is the C–H correlation experiment, which is optimized for long-range magnetization transfer.[3,5–7] The 2D maps obtained with this technique are very useful in establishing the C–C connectivities in the molecule, since they show correlations between ^{13}C and protons that are separated by two or three bonds.

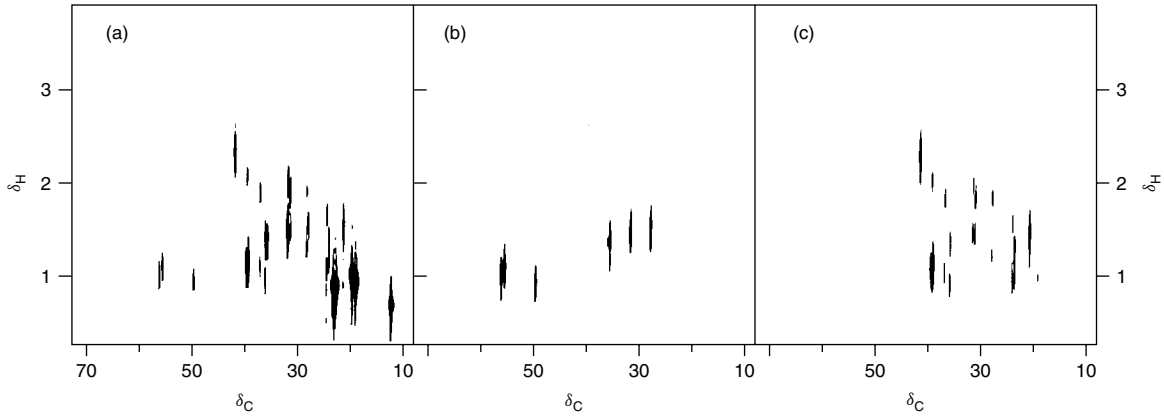

Figure 22.6. Heteronuclear shift correlation maps for cholesterol in $CDCl_3$ at 300 MHz (^{1}H) obtained with the pulse sequence in Figure 22.2(f): (a) transform of FID(30°) showing correlations for CH, CH_2, and CH_3 groups; (b) transform of FID(90°) showing correlations for CH fragments; (c) transform of FID(150°) − FID(30°) containing correlations for CH_2 fragments.

The most obvious approach is to use the pulse sequence in Figures 22.2(c), (d), or (e), and set the lengths of the delays Δ_1 and Δ_2 so that maximum signals would be obtained for carbon–proton spin–spin couplings, $J_{CH}^{\text{long range}}$, of 4–10 Hz. This approach (the COLOC sequence) works well only for isolated spin systems where the carbon atom experiences only long range couplings.[3] In all other cases, the long range correlation peak intensities are modulated by factors $\cos^n(\pi\ {}^1J_{CH}\Delta_2)$, where n is the number of protons directly bonded to a particular carbon atom. This modulation arises from spin–spin interactions between the ^{13}C nucleus and its directly bonded protons during Δ_2. This deficiency can be rectified by inserting a BIRD element at the center of the Δ_2 delay to decouple the directly bonded protons as shown in the pulse sequence in Figure 22.2(g).[3] With this sequence, there is no anomalous modulation of the long-range peaks by directly bonded C–H couplings during Δ_2. The long-range heteronuclear shift correlation map of norharmane shown in Figure 22.7 contains a multitude of correlations over three bonds (e.g., C_{4a}–H_1), and a few two-bond correlations (e.g., C_4–H_3). Analysis of these correlations, together with the ^1H spectrum and the normal heteronuclear correlation map, allows one to establish the structure of the norharmane molecule unambiguously.

It is desirable to suppress all directly bonded correlations from long-range heteronuclear correlation maps as effectively as possible. The BIRD element in the center of Δ_2 significantly decreases the intensities of directly bonded correlations, but the suppression is often incomplete, particularly for compounds with a wide range of $^1J_{CH}$. A number of approaches have been used to improve the suppression efficiency. Satisfactory suppression is obtained by inserting a two step J-filter element, $-1/(2^1J_{CH}) - 90^\circ_{^{13}C} - 1/(2^1J_{CH}) - 90^\circ_{^{13}C}-$, directly after the initial $90^\circ_{^1H}$ pulse in the long range heteronuclear correlation sequence given in Figure 22.2(g) (the BIRDTRAP sequence).[15] An alternate approach to suppression of directly bonded correlations and improved sensitivity in long-range heteronuclear correlation spectroscopy is embodied in the FLOCK sequence, in which the $180^\circ_{^{13}C}$ pulse at the center of the t_1 labeling period is replaced by a BIRD element to effect ^1H–^1H decoupling during t_1, and a third BIRD element is placed at the center of the Δ_1 period.[3] The presence of such a large number of pulses in FLOCK makes it more sensitive to the effects of rf inhomogeneity and offset than the sequence in Figure 22.2(g).

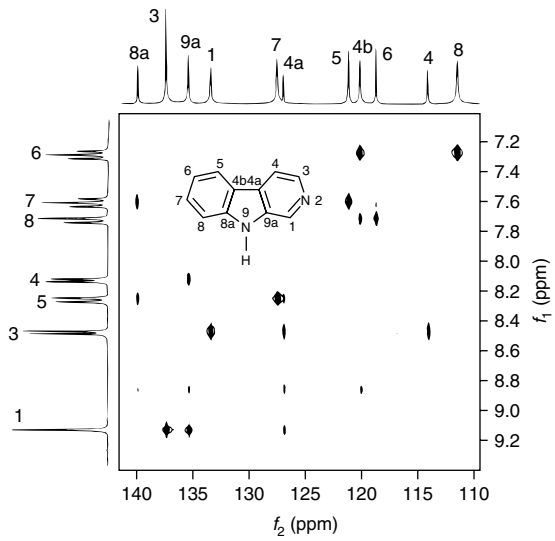

Figure 22.7. Long-range heteronuclear shift correlation map for norharmane in DMSO-d_6 at 300 MHz (^1H) obtained with the BIRDTRAP sequence,[15] a version of the pulse sequence in Figure 22.2(g) that contains a two-step J filter after the initial proton pulse.

22.3.3 Inverse Detection: HSQC and HMQC

In the preceding sections, we have described only heteronuclear shift correlation experiments in which proton magnetization is excited and transferred to carbon for detection. The overall sensitivity of a 2D NMR experiment is proportional to $\gamma_e\gamma_d^{3/2}$, where γ_e is the magnetogyric ratio for the nucleus excited by the initial pulse and γ_d is the magnetogyric ratio of the nucleus whose magnetization is detected. Since $\gamma_{^1H} \approx 4\gamma_{^{13}C}$, the conventional ^1H–^{13}C heteronuclear shift correlation experiment is about 8 times less sensitive than 2D experiments in which proton magnetization is excited and detected.[1] This implies that the overall sensitivity of heteronuclear shift correlation spectroscopy could be improved by a factor of eight if the pulse sequence were modified so that "inverse" (i.e. proton rather than carbon) detection could be employed.

There are a number of *technical* problems associated with the design of heteronuclear shift correlation experiments in which proton magnetization is detected:

1. The spectrometer, probe and control software must have full multichannel rf capabilities so

that one can pulse ^{1}H and ^{13}C, and detect ^{1}H magnetization while performing ^{13}C decoupling. Until recently, the rf hardware in most spectrometers was designed to perform ^{13}C spectroscopy by applying ^{13}C pulses and detecting ^{13}C signals through a "transmitter" coil, and applying ^{1}H pulses through a "decoupler" coil. Modern spectrometers now provide capabilities for pulsing, decoupling, and/or observing on each of two or more independent rf channels, and the control software implements "inverse" detection with ease. A further improvement in sensitivity is achieved by using an "inverse" probe, which is designed with the ^{1}H coil wound closest to the sample for maximum detected ^{1}H signal.

2. One must be able to decouple ^{13}C efficiently while sampling the ^{1}H magnetization. This is a very demanding requirement, since the ^{13}C spectral bandwidth is much larger than the ^{1}H bandwidth, so that ^{13}C decoupling using conventional methods requires much higher decoupler power levels than those used in ^{1}H decoupling. The recent development of GARP[16] now affords very effective ^{13}C decoupling over wide bandwidths at much lower power levels than conventional methods.
3. One must selectively detect signals associated with protons in $^{13}CH_n$ fragments, while suppressing the ^{1}H signals associated with protons in $^{12}CH_n$ fragments. This can be very difficult, since the natural abundance of ^{13}C is only 1.1%, so one must suppress signals that may be 100 times more intense than the desired signals. One encounters severe dynamic range problems if one attempts to use a simple difference technique to eliminate the large signals from the $^{12}CH_n$ protons. The dynamic range problem has been overcome, and excellent selectivity has been achieved by the development of suitable pulse sequences to achieve the necessary signal suppression.[17] The sensitivity of "inverse" heteronuclear shift correlation experiments has also been improved dramatically by the use of pulsed field gradients.

In addition to these technical problems, the realization of a heteronuclear shift correlation experiment with ^{1}H detection required the development of robust pulse sequences to manipulate the proton magnetization in order to obtain the necessary labeling of the magnetization with ^{13}C{^{1}H} frequencies during t_1 and ultimately acquire a ^{1}H{^{13}C} FID.[17] The most straightforward approach is to use INEPT to convert proton magnetization to carbon,[11] allow it to precess and become labeled with carbon frequencies during t_1 (applying a 180° proton pulse at the center of t_1 to remove ^{13}C–^{1}H coupling), then convert the carbon magnetization back to proton magnetization (reverse INEPT) for detection, and finally collect the proton FID while applying GARP carbon decoupling.[16] This heteronuclear single quantum correlation (HSQC) sequence is shown in Figure 22.8(a).[17]

In order to suppress the magnetization from protons in $^{12}CH_n$ fragments, it is important to precede the proton excitation pulse by a BIRD suppression sequence[7]

$$90^\circ_{x\,^1\mathrm{H}} - 1/(2^1J_{\mathrm{CH}}) - 180^\circ_{^{13}\mathrm{C}},\ 180^\circ_{x\,^1\mathrm{H}} - 1/(2^1J_{\mathrm{CH}}) - 90^\circ_{-x\,^1\mathrm{H}} - \Delta \qquad (22.7)$$

This BIRD element inverts the longitudinal magnetization from protons in $^{12}CH_n$ fragments, but the magnetization from protons in $^{13}CH_n$ groups is not inverted. The $^{12}CH_n$ proton z magnetization is then allowed to relax to zero during the delay period Δ so that it gives no transverse magnetization when the following 90° proton pulse is applied, thereby avoiding any potential dynamic range problems. For macromolecules that exhibit negative NOEs, this approach to selective saturation should be avoided, because cross relaxation between the inverted magnetization of the remote protons and the noninverted magnetization of the directly bonded protons during the Δ delay leads to decreased signals from the directly bonded protons.[17]

A different approach for obtaining heteronuclear shift correlation maps using inverse detection involves the creation of multiple quantum coherences (^{1}H–^{13}C zero and double quantum coherences) and the manipulation of these coherences during the evolution period so that they become labeled with carbon frequencies (see also Chapter 17). This heteronuclear multiple quantum coherence (HMQC) technique requires far fewer pulses than HSQC, as shown in the pulse sequence in Figure 22.8(b).[17] As in HSQC, selective saturation of $^{12}CH_n$ proton magnetization is used to suppress the large signals from the $^{12}CH_n$ protons. The proton 90° pulse following the BIRD sequence creates transverse magnetization derived only from protons in $^{13}CH_n$ groups, which is converted to antiphase magnetization during the τ delay period, then transformed into zero quantum coherence (ZQC) and double quantum coherence (DQC) by the 90° carbon pulse. The ZQC precesses at frequency

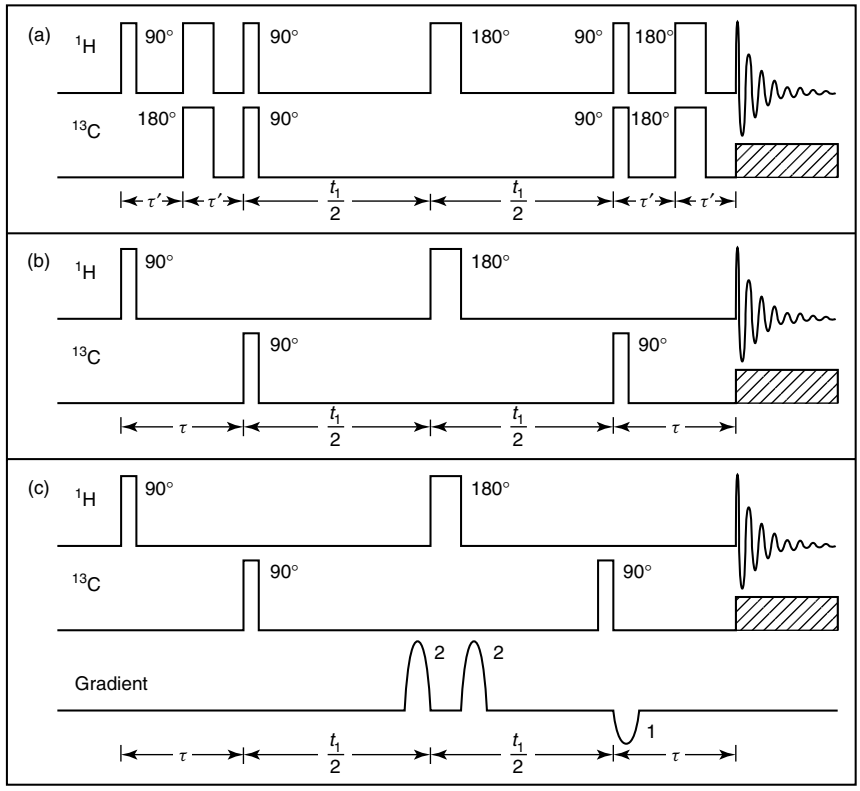

Figure 22.8. Pulse sequences for 'inverse' heteronuclear shift correlation experiments: (a) HSQC, (b) HMQC, and (c) PFG–HMQC. In sequence (a), $\tau' = 1/(4\ ^1J_{CH})$. In sequences (b) and (c), $\tau = 1/(2\ ^1J_{CH})$. In implementing sequences (a) and (b), a BIRD selective presaturation sequence should precede the first proton pulse.

$\nu_C - \nu_H$ and the DQC precesses at frequency $\nu_C + \nu_H$ during the evolution period. The proton 180° pulse at the center of the evolution period interchanges the ZQC and DQC, so that the coherence that had precessed at frequency $\nu_C + \nu_H$ during the first half of the evolution period now evolves at frequency $\nu_C - \nu_H$ and vice versa, so that, at the end of the evolution period, both multiple quantum coherences will be labeled with phase factor $\exp(2\pi i \nu_C t_1)$. The labeled multiple quantum coherences are transformed into antiphase proton magnetization by the 90° carbon pulse. This antiphase magnetization is converted to in-phase magnetization by ^{13}C–^{1}H coupling during the delay τ so that GARP carbon decoupling can be applied while the proton FID is acquired.[16] Long range ^{1}H–^{13}C correlations can also be observed using inverse detection (heteronuclear multiple bond correlation or HMBC).[17]

It should be noted that ^{1}H–^{1}H coupling is present in HMQC maps, but not in HSQC maps. This implies that HSQC should have superior sensitivity and resolution. On the other hand, HSQC has many more rf pulses, and is therefore much more susceptible to pulse imperfections than HMQC. Increased sensitivity and resolution may be obtained by combining the HSQC and HMQC sequences into the HSMQC sequence.[17]

22.3.4 Pulsed Field Gradients: PFG–HMQC

HMQC and HSQC experiments provide excellent heteronuclear shift correlation maps in most cases, but they require the use of phase cycling to suppress signals from protons attached to ^{12}C, and dynamic range problems in analog-to-digital signal conversion

can degrade the overall sensitivity. The application of pulsed field gradients at appropriate points in the HMQC or HSQC pulse sequence gives very effective suppression of the signals from protons attached to ^{12}C and those from solvent molecules. Furthermore, the acquisition of only a single transient for each value of t_1 is often sufficient to produce a heteronuclear shift correlation map of high quality, since the applied gradients divert the unwanted signals so that they never reach the detector and need not be canceled by phase cycling. An HMQC pulse sequence employing pulsed field gradients (PFG–HMQC) is shown in Figure 22.8(c). In the PFG–HMQC sequence,[18] field gradients of the same phase and length are applied immediately before and after the proton 180° pulse at the center of the evolution period, and a gradient of smaller magnitude and opposite phase is applied immediately after the final carbon 90° pulse. The first field gradient pulse attaches a phase factor $\exp[i(\gamma_C - \gamma_H)zG_1\tau_1]$ to the ZQC and a phase factor $\exp[i(\gamma_C + \gamma_H)zG_1\tau_1]$ to the DQC. Here z is the vertical position of the molecule in the sample, G_1 is the intensity of the field gradient, and τ_1 is the duration of the field gradient pulse. The coherences in different parts of the sample now have different phases. When the proton 180° pulse is applied, the ZQC and DQC are interchanged, so that the application of the second field gradient pulse (which has the same intensity and duration as the first gradient pulse) results in phase factors of $\exp(2i\gamma_C zG_1\tau_1)$ being attached to both ZQC and DQC. When these multiple quantum coherences are converted to antiphase proton magnetization by the final carbon pulse, this magnetization is labeled with the gradient phase factor $\exp(2i\gamma_C zG_1\tau_1)$, and protons in molecules at different points in the sample have different phases. The refocusing of the disperse magnetization elements is achieved by applying a field gradient pulse of intensity G_2 and duration τ_2, which attaches a phase factor $\exp(2i\gamma_H zG_2\tau_2)$ to the antiphase proton magnetization. By choosing $G_2\tau_2 = -2G_1\tau_1\gamma_C/\gamma_H \approx -{}^1/_2G_1\tau_1$, the net effects of the pulsed field gradients on the desired magnetizations will be removed, and the antiphase proton magnetizations in all parts of the sample will have the same phase. The magnetizations from the solvent protons and from protons in $^{12}CH_n$ fragments are completely dephased by the gradient pulses.

The heteronuclear shift correlation map for sucrose obtained using the HMQC sequence with a minimum four-step phase cycle is compared in Figure 22.9 with the corresponding PFG–HMQC map obtained by acquiring only a single FID for each t_1. The HMQC map contains a relatively intense water "stripe" due

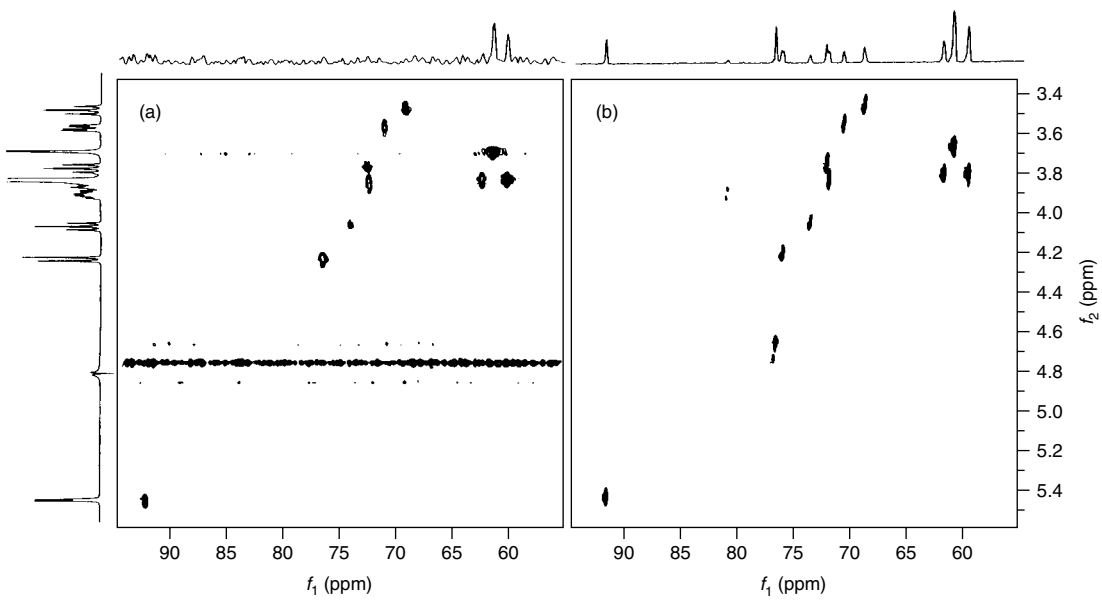

Figure 22.9. HMQC (a) and PFG–HMQC (b) heteronuclear correlation maps for sucrose in D_2O (10 mg in ≈0.5 mL) at 500 MHz (^1H). Four FIDs were accumulated per t_1 value in (a), but only a single FID per t_1 value was acquired in (b).

to the incomplete subtraction of the large water signals in alternate FIDs. The projection of the HMQC map onto the ^{13}C axis is virtually useless, since it is totally dominated by the t_1 ridge of the water signal, but the individual carbon slices are useful. Because of the coherence pathway selection afforded by the pulsed field gradients, the water signal never reaches the receiver in the PFG–HMQC experiment, so the PFG–HMQC map has no water ridge. Furthermore, since one can use higher receiver gain in PFG–HMQC and achieve full digitization of the small signals of interest, the sensitivity of PFG–HMQC is higher, as evidenced by the observation of the weak C–H correlation peak for the F5 center of sucrose in the PFG–HMQC map, but not in the HMQC map. Thus, PFG–HMQC is faster and more sensitive than HMQC. Note that, because only one transient is acquired per t_1 value, any mismatch in the quadrature detectors may produce a transmitter glitch at the center of f_2, as shown in Figure 22.9(b). Acquisition of more than a single transient for each t_1 will suppress this artifact. Further improvements in sensitivity and resolution can be achieved with phase-sensitive versions of PFG–HMQC and PFG–HSQC.[19]

RELATED ARTICLES IN THE ENCYCLOPEDIA OF MAGNETIC RESONANCE

Carbon-13 Relaxation Measurements: Organic Chemistry Applications

Decoupling Methods

Field Gradients and Their Application

Fourier Transform Spectroscopy

Heteronuclear Assignment Techniques

INEPT

Inorganic Nuclei: Low Sensitivity Transition Metals

Natural Products

Organic Chemistry Applications

Phase Cycling

Polarization Transfer Experiments via Scalar Coupling in Liquids

Radiofrequency Pulses: Response of Nuclear Spins

Spectrometers: A General Overview

REFERENCES

1. R. R. Ernst, G. Bodenhausen, and A. Wokaun, *Principles of Nuclear Magnetic Resonance in One and Two Dimensions*, Oxford University Press, Oxford, 1987, Chap. 8
2. A. E. Derome, *Modern NMR Techniques for Chemistry Research*, Pergamon Press, Oxford, 1987, Chap. 9
3. G. E. Martin and A. S. Zektzer, *Two-Dimensional NMR Methods for Establishing Molecular Connectivity: A Chemist's Guide to Experiment Selection, Performance and Interpretation*, VCH, New York, 1988, Chap. 3
4. A. Bax, *Two-Dimensional Nuclear Magnetic Resonance in Liquids*, Delft University Press/Reidel, Dordrecht, 1982, Chap. 2
5. W. S. Brey, in *Pulse Methods in 1D and 2D Liquid-Phase NMR*, ed. W. S. Brey, Academic Press, San Diego, 1988, Chap. 1
6. G. A. Gray, in *Pulse Methods in 1D and 2D Liquid-Phase NMR*, ed. W. S. Brey, Academic Press, San Diego, 1988, Chap. 5
7. W. E. Hull, in *Two-Dimensional NMR Spectroscopy: Applications for Chemists and Biochemists*, eds. W. R. Croasmun and R. M. K. Carlson, VCH, New York, 2nd edn., 1994, Chap. 2
8. J. K. M. Sanders and B. K. Hunter, *Modern NMR Spectroscopy. A Guide for Chemists*, Oxford University Press, Oxford, 1987, Chap. 4
9. H-O. Kalinowski, S. Berger, and S. Braun, *Carbon-13 NMR Spectroscopy*, Wiley, Chichester, 1988, Chap. 2
10. R. R. Ernst, G. Bodenhausen, and A. Wokaun, *Principles of Nuclear Magnetic Resonance in One and Two Dimensions*, Oxford University Press, Oxford, 1987, Chap. 4
11. A. E. Derome, *Modern NMR Techniques for Chemistry Research*, Pergamon Press, Oxford, 1987, Chap. 6
12. O. W. Sørensen and H. J. Jakobsen, in *Pulse Methods in 1D and 2D Liquid-Phase NMR*, ed. W. S. Brey, Academic Press, San Diego, 1988, Chap. 3
13. R. R. Ernst, G. Bodenhausen, and A. Wokaun, *Principles of Nuclear Magnetic Resonance in One and Two Dimensions*, Oxford University Press, Oxford, 1987, Chap. 2
14. R. R. Ernst, G. Bodenhausen, and A. Wokaun, *Principles of Nuclear Magnetic Resonance in One and Two*

Dimensions, Oxford University Press, Oxford, 1987, Chap. 6

15. A. M. Torres, T. T. Nakashima, and R. E. D. McClung, *J. Magn. Reson.*, 1992, **96**, 103.
16. A. J. Shaka, P. B. Barker, and R. Freeman, *J. Magn. Reson.*, 1985, **64**, 547.
17. G. E. Martin and R. C. Crouch, *J. Nat. Prod.*, 1991, **54**, 1.
18. R. E. Hurd and B. K. John, *J. Magn. Reson.*, 1991, **91**, 648.
19. G. Wider and K. Wüthrich, *J. Magn. Reson., Ser. B*, 1993, **102**, 239. L. E. Kay, P. Keifer, and T. Saarinen, *J. Am. Chem. Soc.*, 1992, **114**, 10 663. Y-C. Li and G. T. Montelione, *J. Magn. Reson., Ser. B*, 1993, **101**, 315.